

Binary Inspirals in Nordström’s Second Theory

Travis M. Garrett*

Perimeter Institute for Theoretical Physics, Waterloo, Ontario N2L 2Y5, Canada

(Dated: August 18, 2024)

We investigate Nordström’s second theory of gravitation, with a focus on utilizing it as a testbed for developing techniques in numerical relativity. Numerical simulations of inspiraling compact star binaries are performed for this theory, and compared to the predictions of semi-analytic calculations (which are similar to Peters and Mathews’ results for GR). The simulations are based on a corotating spherical coordinate system, where both finite difference and pseudo-spectral methods are used. We also adopt the “Hydro without Hydro” approximation, and the Weak Radiation Reaction approximation when the orbital motion is quasi-circular. We evolve a binary with quasi-circular initial data for hundreds of orbits and find that the resulting inspiral closely matches the 1/4 power law profile given by the semi-analytical calculations. We additionally find that an eccentric binary circularizes and precesses at the expected rates. The methods investigated thus provide a promising line of attack for the numerical modeling of long binary inspirals in general relativity.

I. INTRODUCTION

Numerical methods capable of modeling the strong gravitational fields of merging black holes and neutron stars were found several years ago after many years of searching. The main techniques are centered around the BSSN (see [1–5]) and Generalized Harmonic (GH) formulations [6, 7] of general relativity. These two classes of techniques generally agree in their predictions [8],[9], and also match the Post-Newtonian calculations during the inspiral [10]. We are designing our own numerical relativity techniques for comparable mass binaries with the goal of modeling long stretches of the inspiral phase preceding the merger (as could be useful in discriminating neutron star equations of state [11]). We employ corotating spherical coordinate systems to this end, as they are well adapted to the slow evolution of the binary during this phase. This is similar to the approach of the Caltech group ([12–14]) although we differ in most of the details.

Spherical coordinate systems have several attractive features from a computational standpoint. A spherical mesh has a high density of grid points near the origin where it is needed to resolve the high curvature potential wells of the compact bodies. This thus provides an alternative to the Adaptive Mesh Refinement methods (see e.g. [15],[16]) which have seen success lately. Additionally, a spherical grid provides a S^2 outer boundary, which is more suited to outgoing waves than a cubic grid. One of the key features is that it allows for the use of pseudo-spectral methods: by using spherical harmonics the 3+1 problem can be split into a set of 1+1 problems which can be solved with fast and accurate implicit methods. The usage of spherical harmonics likewise avoids the complications due to the coordinate singularities in θ and ϕ . A spherical system also meshes nicely with corotating coordinates, as proposed in [17]. This removes most of the dynamical motion in the grid, thus helping to cut down

on spurious field excitations.

We are currently supplementing this primary numerical method with some useful additional approximations. Neutron star like compact bodies are our focus, and thus the complications of modeling black holes are avoided. Furthermore we make use of the “Hydro-without-Hydro” approximation [18] so that a relativistic fluid dynamics code is not currently needed. Radial profiles for isolated polytropic stars are generated and then inserted into a binary system. The gravitational fields and net accelerations of the stars in the binary are evolved, while the radial density profiles of the stars are held constant. This is a good approximation as geodesic deviations due to tidal distortions of the stars only arise at high post-Newtonian order.

Another useful approximation is possible when the stars are in quasi-circular orbit (which is generally the case for astrophysical binaries as the gravitational radiation circularizes the orbit). As pointed out in [17], in a corotating coordinate system a quasi-circular binary evolves at the slow radiation reaction time scale $\tau \sim d^4/M^3$ for a separation d and mass M . This makes the Weak Radiation Reaction (WRR) approximation possible: the second time derivatives in the field equations can be dropped, thus changing the character of the differential equations.

There are some numerical drawbacks to using spherical coordinate systems. A primary one is that spherical harmonic decomposition and synthesis are computationally expensive. For instance the decomposition:

$$A_{lm}(r) = \int f(r, \theta, \phi) Y_{lm}^*(\theta, \phi) d\Omega \quad (1)$$

is an $\mathcal{O}(N^5)$ calculation if discretized in a direct manner, although this can be reduced to $\mathcal{O}(N^4)$ by defining intermediate variables and splitting the integration into two steps. The computational cost is further reduced in our case as we only need decompose and synthesize in the small volumes containing our compact bodies. This makes it possible to run high resolution meshes in a reasonable amount of time on a single computer. Further

*Electronic address: tgarrett@perimeterinstitute.ca

reduction the the order of these operations is also possible: [19–21], although these methods have a large amount of overhead and only become efficient for large values of l and m .

There are some other subtle issues that arise in spherical coordinate systems. For instance when using second order accurate methods one finds that very fine meshes are needed to accurately compute the accelerations of the stars. We find that using higher order methods allows for accurate results with much lower resolution. This is described in greater detail in section 3.

Before we attempt to use these techniques in a full GR code we have elected to test them in a scalar gravity model theory (following the advice of [22] and [23]). This forms the focus of this paper. After the tests are successful we can then feel confident in applying the methods to a full general relativistic code. After considering several scalar theories, we chose Nordström’s second theory (see [24]). It is a fully conservative metric theory, with parameterized post-Newtonian parameters $\gamma = -1$, $\beta = 1/2$ and all others zero. The theory thus has no Nordtvedt effect (see [25]), and the stars move on Keplerian orbits in the limit of small mutual gravitational potential. This is nontrivial since the Nordtvedt effect can produce considerable deviation from Keplerian orbits for highly compact bodies, even at arbitrarily large separations. We can therefore perform a semi-analytic calculation of the rate of energy and angular momentum loss for a binary based on the Keplerian motion, in a similar fashion to Peters and Mathews’ calculation in GR ([26],[27]). We find that the radiation is quadrupole to the leading order, despite being based on scalar field, due to approximate conservation of mass and momentum.

The fully conservative nature of Nordström’s theory has an additional benefit in that it justifies the use of the “Hydro-without-Hydro” approximation. The approximation is safe since corrections to the star’s equilibrium do not show up through first post-Newtonian order for fully conservative theories [28].

In the following sections we first review the details of Nordström’s second theory. We describe the construction of isolated stars in this theory, and the equations of motion for the matter. We then review the 1PN equations of motion, which lead to precession for eccentric binaries. We calculate the energy and angular momentum loss on a large S^2 in the wave zone, and apply the results to a Keplerian system, which cause the binary to decay and circularize in a similar fashion to GR. Next we detail the numerical methods used to simulate the binary, including switching to a co-rotating reference frame, and several preliminary test cases that are needed to check the performance of the code. We finish with the results of simulating Nordström binaries in both quasi-circular and slightly eccentric orbits.

We obtain a nice agreement between our simulation and the analytic calculations. The orbital decays of quasi-circular and eccentric binaries closely match the expectations from our semi-analytic calculations, as seen

in the evolution of the semi-major axis a and eccentricity e . We also find that the eccentric binaries precess at the rate predicted by 1st Post Newtonian calculations, which gives supporting evidence that Nordström’s theory obeys the Strong Equivalence Principle (SEP).

II. NORDSTRÖM’S SECOND THEORY

After the development of special relativity it became clear that Newton’s gravitational theory could no longer be completely correct. For instance the Poisson equation is solved simultaneously throughout all of space, and thus the acceleration of a massive body would allow for the instantaneous transmission of signals, in disagreement with the finite speed of light. Comparisons with electromagnetic theory suggested that the spatial Laplacian operator should be replaced with the D’Alembertian wave operator. Gunnar Nordström used this idea to develop two relativistic scalar gravity theories a couple years before Einstein discovered General Relativity (we focus on the second, more complete theory). Nordström’s theory is not a viable candidate for describing relativistic gravitation, as Nordström quickly realized after Einstein presented his tensor theory. For instance, being conformally flat, it predicts zero bending of light. However, it does provide an excellent arena for developing tools for numerical relativity.

Einstein and Fokker demonstrated that Nordström’s second theory could be expressed in geometric terms. The metric is conformally flat (thus the Weyl tensor is zero: $C_{\alpha\beta\gamma\delta} = 0$) and is specified by a scalar field φ :

$$g_{\mu\nu} = (1 + \varphi)^2 \eta_{\mu\nu}. \quad (2)$$

The scalar field is generated in turn by setting the Ricci scalar to be equal to the trace of the stress energy tensor (see [24]):

$$R = 24\pi T. \quad (3)$$

For our simulations we will use the standard perfect fluid stress energy tensor:

$$T^{\mu\nu} = (\rho + p)u^\mu u^\nu + g^{\mu\nu} p, \quad (4)$$

so the field equation becomes:

$$\square\varphi = 4\pi(1 + \varphi)^3(\rho + p - 3p). \quad (5)$$

Being conformally flat, Nordström’s theory effectively has a background geometry $\eta_{\mu\nu}$, and a conserved energy-momentum complex can be constructed:

$$t^{\mu\nu} = \frac{1}{4\pi} \left[\eta^{\mu\alpha} \eta^{\nu\beta} \varphi_{,\alpha} \varphi_{,\beta} - \frac{1}{2} \eta^{\mu\nu} \eta^{\alpha\beta} \varphi_{,\alpha} \varphi_{,\beta} \right] + (1 + \varphi)^6 T^{\mu\nu}, \quad (6)$$

with $t^{\mu\nu}{}_{,\nu} = 0$. Nordström’s theory has gravitational waves, although they are different from those in general relativity since $C_{\alpha\beta\gamma\delta} = 0$. Namely, the waves

occur in the scalar field φ as described by equation (5), and (6) describes their localizable energy density: $t^{00} = (1/8\pi)[(\partial_t\varphi)^2 + (\nabla\varphi)^2]$.

A. Single Star Solution

We utilize the hydro-without-hydro approximation in our code. This is a good approximation since tidal distortions of the stars do not affect the orbital dynamics until relatively high Post-Newtonian order. We thus need to construct a model of a single star in Nordström's theory to use as a source in the main code. For a single isolated star equation (5) becomes:

$$\frac{1}{r^2}\partial_r(r^2\partial_r\varphi) = 4\pi(1+\varphi)^3[\rho(1+\varepsilon) - 3p]. \quad (7)$$

We will assume the star is a polytrope, so that the pressure and internal energy are given by:

$$p = \kappa\rho^\Gamma, \quad (8)$$

$$\varepsilon = \frac{\kappa}{\Gamma-1}\rho^{\Gamma-1}, \quad (9)$$

which reduces equation (7) to two variables. Application of the projection operator $Q_\mu^\alpha = u^\alpha u_\mu + \delta_\mu^\alpha$ on the divergence of the stress energy tensor $T^{\mu\nu}{}_{;\mu} = 0$ gives:

$$\rho h u^\nu u^\alpha{}_{;\nu} + Q^{\alpha\nu} p_{,\nu} = 0 \quad (10)$$

where h is the relativistic specific enthalpy: $h = h(\rho) = 1 + \varepsilon + p/\rho$. With $u^0 = 1/(1+\varphi)$ and $u^i = 0$ this reduces this to:

$$\frac{d\varphi}{dr} = -\frac{(1+\varphi)}{h} \frac{dh}{dr}. \quad (11)$$

We solve (7) and (11) iteratively. In the first iteration the $(1+\varphi)^3$ and $(1+\varphi)$ terms are dropped respectively, resulting in a modified Lane-Emden equation which is solved by specifying the central pressure ρ_c and integrating out. For successive iterations the $(1+\varphi)^3$ and $(1+\varphi)$ terms are reinserted with the previous iteration's solution for φ . The iterative process converges for values of ρ_c below some critical value (which depends on κ and Γ). For instance, with a stiff equation of state with $\Gamma = 2$ we find the most compact star that can be formed has radius $R \sim 1.75M$, which is smaller than the event horizon radius in classical GR (in addition to being smaller than the Buchdahl-Bondi bound of $R = 9/4M$ for GR). We use the softer value of $\Gamma = 5/3$ to generate stars for the simulation, as the smoother transition to zero density at the outer boundary of the star allows the spherical harmonic decomposition to converge more quickly.

B. Matter Equations of Motion

The isolated star solutions will be used in the binary simulation with the hydro-without-hydro approximation,

so that only the net accelerations of the centers of masses need to be found. The conserved density ρ^* (see [29]) proves useful to this end:

$$\rho^* = \rho(-g)^{1/2}u^0 = \rho\frac{(1+\varphi)^3}{\sqrt{1-v^2}}, \quad (12)$$

with $\partial_t\rho^* + \partial_i(\rho^*v^i) = 0$. The conserved density can be used to define the center of mass for star a :

$$x_a^j = \frac{1}{M_a^*} \int_a \rho^* x^j d^3x, \quad (13)$$

where M_a^* is volume integral of ρ^* . Differentiating twice gives the coordinate acceleration a_a^i of the center of mass:

$$a_a^j = \frac{1}{M_a^*} \int_a \rho^* \frac{dv^j}{dt} d^3x. \quad (14)$$

An expression for the local accelerations dv^j/dt is then found by expanding the projection of the divergence of the stress energy tensor (10):

$$\begin{aligned} \rho^* \frac{dv^j}{dt} = & -\rho^* \Gamma_{\alpha\beta}^j v^\alpha v^\beta - (u^0)^{-1} \rho^* v^j \frac{du^0}{dt} \\ & - (u^0)^{-2} \frac{\rho^*}{\rho h} Q^{j\nu} p_{,\nu}. \end{aligned} \quad (15)$$

During the simulation the terms in (15) are calculated and integrated with (14) to find the net acceleration of the star (with the radial profile for ρ^* kept constant).

C. Semi-Analytical Calculation of Orbital Evolution

Semi-analytic calculations of the evolution of a binary system in Nordstrom's theory are needed so that comparisons can be made with the numerical simulations. We first review the 1PN results for the theory, which follow from having the parameterized post-Newtonian parameters given by $\gamma = -1$, $\beta = 1/2$ (and all others zero). The theory therefore has no Nordtvedt effect (since $4\beta - \gamma - 3 = 0$ - see [29]) and compact stars move on Keplerian orbits at large separations. The 1PN analysis also leads to precession for eccentric binaries. Next we will solve for the energy and angular momentum radiated at large radius by a binary on a Keplerian orbit, and then apply these results to evolve the orbital parameters.

Consider first a binary with stars a and b in a slightly eccentric orbit with an angular velocity ω . Arrange a Cartesian coordinate system so that the binary is instantaneously aligned along the x -axis, with a separation d and the bulk of the velocity in the \hat{y} direction: $v_a^y \sim \omega d/2$, and a small amount of radial velocity v_a^x . The PN analysis then finds that the acceleration \ddot{x}_a of star a in the \hat{x} direction is:

$$\ddot{x}_a = -\frac{M_b}{d^2} \left(1 + \frac{M_b}{d} - v_a^2 - \frac{3}{2}(v_b^x)^2 - (v_a^x - v_b^x)v_b^x \right), \quad (16)$$

where $M_b = \int_b \rho^* (1 + (1/2)\bar{v}^2 - (1/2)\bar{U} + \varepsilon) d^3x$ is the gravitational mass (equal to the inertial mass) of star b (with $\bar{U} = \int_b \rho' |\mathbf{x} - \mathbf{x}'|^{-1} d^3x'$ and $\bar{\mathbf{v}} = \mathbf{v} - \mathbf{v}_0$ where \mathbf{v}_0 is velocity of the center of mass). The acceleration in the \hat{y} direction is:

$$\ddot{y}_a = \frac{M_b(v_a^y - v_b^y)v_b^x}{d^2}. \quad (17)$$

At large separations the post-Newtonian corrections M_b/d and v_a^2 drop out, leaving the binary in a Keplerian orbit. This confirms that Nordström's second theory has no Nordtvedt effect through 1PN order (and as a purely geometric theory it should follow the SEP). One further consequence of the post-Newtonian corrections (16) and (17) is that an eccentric binary will precess. A binary with semi-major axis a , eccentricity e , and total mass M will precess $\Delta\tilde{\omega}$ radians per orbit [29]:

$$\Delta\tilde{\omega} = -\frac{\pi M}{a(1-e^2)}. \quad (18)$$

This is six times slower and in the opposite direction as GR.

D. Energy Loss at Outer Boundary

We next find the energy radiated by a binary due to the waves generated in φ . The energy-momentum complex 6 follows the standard flat-space conservation law:

$$t^{\mu\nu}{}_{,\nu} = 0. \quad (19)$$

Integration inside a volume bounded by S^2 gives:

$$\int t^{00}{}_{,0} d^3x = - \int t^{0i}{}_{,i} d^3x, \quad (20)$$

or, using Gauss's law:

$$\partial_t E = - \int t^{0i} n_i dS. \quad (21)$$

with t^{0i} given by:

$$t^{0i} = -\frac{1}{4\pi} \partial_t \varphi \partial_i \varphi. \quad (22)$$

The spatial derivative $\partial_i \varphi$ can be transformed into $-n^i \partial_t \varphi$ since at large radius φ is approximately a spherical wave: $\varphi \sim \sin(t-r)/r$. This leads to:

$$\partial_t E = -\frac{1}{4\pi} \int (\partial_t \varphi)^2 r^2 d\Omega \quad (23)$$

for the energy loss.

An expression for $\partial_t \varphi$ is needed next. Rewriting the equation of motion for the field (5) with the conserved mass density ρ^* gives:

$$\square \varphi = 4\pi \rho^* (1 - v^2)^{1/2} (1 + \varepsilon - 3p/\rho). \quad (24)$$

This can be solved with a Green's function:

$$\varphi = - \int \frac{[\rho^{*'} (1 - (1/2)v'^2 + \varepsilon' - 3p'/\rho' + \mathcal{O}(v^4))]_{ret}}{|\mathbf{x} - \mathbf{x}'|} d^3x', \quad (25)$$

which is evaluated at the retarded time $t' = t - |\mathbf{x} - \mathbf{x}'|$. The $1/|\mathbf{x} - \mathbf{x}'|$ term expands into:

$$\frac{1}{|\mathbf{x} - \mathbf{x}'|} = \frac{1}{r} + \frac{x^j x^{j'}}{r^3} + \dots \quad (26)$$

Only the first term is needed since it is utilized at large radius. Likewise only the first term in the expansion:

$$r - |\mathbf{x} - \mathbf{x}'| = \frac{x^j x^{j'}}{r} + \frac{x^j x^k (x^{j'} x^{k'} - r'^2 \delta_k^j)}{2r^2} + \dots \quad (27)$$

will be needed. Equation (25) can thereby be expanded out in multipole moments:

$$\varphi = -\frac{1}{r} \left[M + n_i \partial_t D^i + \frac{1}{2} n_i n_j \partial_t^2 Q^{ij} + \dots \right] \quad (28)$$

with

$$M = \int \rho^{*'} (1 - (1/2)v'^2 + \varepsilon' - 3p'/\rho' + \mathcal{O}(v^4)) d^3x', \quad (29)$$

$$D^i = \int \rho^{*'} (1 - (1/2)v'^2 + \varepsilon' - 3p'/\rho' + \mathcal{O}(v^4)) x^{i'} d^3x', \quad (30)$$

and

$$Q^{ij} = \int \rho^{*'} (1 - (1/2)v'^2 + \varepsilon' - 3p'/\rho' + \mathcal{O}(v^4)) x^{i'} x^{j'} d^3x' \quad (31)$$

(and higher multipoles unnecessary for a leading order calculation of the energy loss).

The time derivatives of these multipole moments are needed for (23). The quadrupole contribution $\partial_t^3 Q^{ij}$ scales as v^5 , so all terms of order v^6 and higher will be dropped for this leading order calculation. We first examine the time derivative of the monopole:

$$\partial_t M = \int \rho^{*'} \frac{d}{dt} (1 - (1/2)v'^2 + \varepsilon' - 3p'/\rho') d^3x', \quad (32)$$

where $(d/dt) \int_V \rho^* f d^3x = \int_V \rho^* (df/dt) d^3x$ has been used to pass the time derivative through ρ^* . Note that if the two stars are on a quasi-circular orbit then the time derivatives in the integrand are on the radiation reaction timescale, and thus contribute radiation at a far lower scale than v^5 . However, they do contribute to eccentric binaries where the separation oscillates on the orbital timescale.

First consider the $d\varepsilon/dt$ term in (32), and to simplify assume that $\Gamma = 2$, although the result holds in general. The specific internal energy can be expanded: $\varepsilon = \kappa\rho = \kappa\rho^* (1 - (1/2)v^2 - 3\varphi + \mathcal{O}(v^4))$, where only the first term can contribute through quadrupole order. This

term reduces to $d\varepsilon/dt = -\kappa\rho^*\partial_i v^i$. Thus any monopole radiation of order v^5 from the $d\varepsilon/dt$ term stems from the “breathing” motion as the star expands and contracts during the elliptical orbit. However, Nordström’s second theory is fully conservative, and accordingly the stellar matter undergoes no “breathing” motion: the central density is constant to 1PN order (which justifies the use of the “Hydro-without-Hydro” assumption). Therefore the entire $d\varepsilon/dt$ term does not contribute at v^5 order. The same holds for the $d(3p/\rho)/dt$ term. We find the monopole contribution to the radiation:

$$\partial_t M = -\frac{1}{2} \int \rho^* \partial_t (v^2) d^3 x' + \mathcal{O}(v^7), \quad (33)$$

which is at v^5 order if the orbit is eccentric and is much smaller otherwise (note also that the total time derivative has been switched to a partial derivative since the velocity is now essentially constant throughout the star). Note that it is also convenient that radial pulsations do not contribute at leading order as this allows the stars to be treated as point bodies in later calculations.

We next examine the contribution from the dipole via $\partial_t^2 D^j$. Distributing the two time derivatives through the integrand gives:

$$\begin{aligned} \partial_t^2 D^j &= \int \rho^* [(1 - v^2 + \varepsilon' - 3p'/\rho') \frac{dv^{j'}}{dt} \\ &\quad - \frac{d}{dt} \left(\frac{dv^{i'}}{dt} v^{i'} \right) x^{j'} - 2 \frac{dv^{i'}}{dt} v^{i'} v^{j'}] d^3 x'. \end{aligned} \quad (34)$$

The $\int \rho^* (dv^{j'}/dt) d^3 x'$ term integrates to zero due to Newton’s third law. Any corrections would enter at v^6 order at the soonest, and all the other terms in equation (34) also scale as v^6 . Thus the dipole does not radiate to leading order:

$$\partial_t^2 D^j = 0 + \mathcal{O}(v^6). \quad (35)$$

The final multipole moment that can contribute through leading order is the quadrupole. The $(1/2)v'^2$, ε' , and $-3p'/\rho'$ terms all enter at $\mathcal{O}(v^7)$, leaving only:

$$\partial_t^3 Q^{ij} = \partial_t^3 \int \rho^* x^{i'} x^{j'} d^3 x' + \mathcal{O}(v^7). \quad (36)$$

Combining the terms from the monopole and quadrupole gives:

$$\partial_t E = -\frac{1}{4\pi} \int (\partial_t M + (1/2)n_i n_j \partial_t^3 Q^{ij})^2 d\Omega \quad (37)$$

for the rate of energy loss. With the integrals:

$$\begin{aligned} \int n_i n_j d\Omega &= \frac{4\pi}{3} \delta^{ij}, \quad (38) \\ \int n_i n_j n_k n_l d\Omega &= \frac{4\pi}{15} [\delta_j^i \delta_l^k + \delta_k^i \delta_l^j + \delta_l^i \delta_k^j] \end{aligned}$$

this becomes:

$$\partial_t E = -(\partial_t M)^2 - \frac{1}{3} \partial_t M \partial_t^3 Q^{ii} - \frac{1}{60} (\partial_t^3 Q^{ii})^2 - \frac{1}{30} (\partial_t^3 Q^{ij})^2. \quad (39)$$

This reduces to:

$$\partial_t E = -\frac{1}{30} (\partial_t^3 Q^{ij})^2 \quad (40)$$

for zero eccentricity case, which is six times smaller than the value found in GR.

E. Angular Momentum Loss at Outer Boundary

A similar calculation determines the rate at which the angular momentum is radiated. With equation (19) and:

$$L_i = \epsilon_{ijk} \int x^j t^{0k} d^3 x \quad (41)$$

one finds:

$$\frac{dL_i}{dt} = -\epsilon_{ijk} \int x^j t^{kl}{}_{,l} d^3 x = -\epsilon_{ijk} \int x^j t^{kl} n^l dS. \quad (42)$$

The spatial stress energy tensor components are:

$$t^{kl} = \frac{1}{4\pi} \partial_k \varphi \partial_l \varphi - \frac{1}{8\pi} \delta_l^k \eta^{\alpha\beta} \partial_\alpha \varphi \partial_\beta \varphi, \quad (43)$$

and thus:

$$\frac{dL_i}{dt} = -\frac{1}{4\pi} \epsilon_{ijk} \int x^j \partial_k \varphi \partial_l \varphi n^l dS. \quad (44)$$

The $\eta^{\alpha\beta} \partial_\alpha \varphi \partial_\beta \varphi$ term is zero due to the anti-symmetry of ϵ_{ijk} .

Only one spatial partial derivative should both converted into a time derivative via $\partial_i \varphi = -n^i \partial_t \varphi$:

$$\frac{dL_i}{dt} = -\frac{1}{4\pi} \epsilon_{ijk} \int x^j \partial_k \varphi \frac{1}{r} (\partial_t M + (1/2)n_l n_m \partial_t^3 Q^{lm}) dS, \quad (45)$$

as converting both yields zero due to the anti-symmetry of ϵ_{ijk} (note also that the $n_l \partial_t^2 D^l$ term has been dropped from $\partial_t \varphi$ since it doesn’t contribute at leading order). In particular, examination of ϵ_{ijk} shows that the $\partial_k \varphi$ term that needs to be expanded to higher order, while the $\partial_l \varphi$ can be approximated by the time derivative. Application of the spatial derivative ∂_k to the monopole term in (28) gives:

$$\partial_k \left(-\frac{1}{r} M \right) = \frac{x^k}{r^3} M. \quad (46)$$

Insertion of this term into (45) also gives zero due to the anti-symmetry of ϵ_{ijk} , and the same applies to all terms stemming from derivatives of powers of r . The only remaining relevant terms in $\partial_k \varphi$ are:

$$\partial_k \varphi = -\frac{1}{r^2} \partial_t D^k - \frac{x^l}{r^3} \partial_t^2 Q^{lk} + \dots \quad (47)$$

Upon expansion in (45) the $-\partial_t D^k/r^2$ terms are multiplied by either one or three n^i terms, and as $\int n_i d\Omega = \int n_i n_j n_k d\Omega = 0$ these dipole terms integrate to zero.

Equation (45) thus becomes:

$$\frac{dL_i}{dt} = \frac{1}{4\pi} \epsilon_{ijk} \int n^j n^l \partial_t^2 Q^{lk} (\partial_t M + (1/2) n_a n_b \partial_t^3 Q^{ab}) d\Omega. \quad (48)$$

Reusing the integrals (38) leads to:

$$\frac{dL_i}{dt} = \frac{1}{15} \epsilon_{ijk} \partial_t^3 Q^{jl} \partial_t^2 Q^{lk} \quad (49)$$

where the $\partial_t M$ term has also dropped out, again due to ϵ_{ijk} . This expression is precisely one sixth of the value given by general relativity.

F. Application to Keplerian Orbits

We can now apply the equations for the rates of energy (39) and angular momentum loss (49) to a binary star system in Keplerian orbit. The stars have gravitational masses m_1 and m_2 , a semi-major axis a and eccentricity e . The separation d between the two stars is determined by the phase ϕ :

$$d = \frac{a(1 - e^2)}{1 + e \cos(\phi)}, \quad (50)$$

with the distances of the stars from the center of mass being:

$$d_1 = \left(\frac{m_2}{m_1 + m_2} \right) d, \quad d_2 = \left(\frac{m_1}{m_1 + m_2} \right) d. \quad (51)$$

The non-zero quadrupole moment components are:

$$\begin{aligned} Q_{xx} &= \mu d^2 \cos^2 \phi, \\ Q_{yy} &= \mu d^2 \sin^2 \phi, \\ Q_{xy} &= Q_{yx} = \mu d^2 \sin \phi \cos \phi \end{aligned} \quad (52)$$

with $\mu = m_1 m_2 / (m_1 + m_2)$. Note that the Q_{ij} are expressed here in terms of the gravitational mass instead of the conserved mass $m^* = \int \rho^* d^3x$ as used in the previous section. Switching between the two involves corrections of order v^2 which do not affect the leading order calculation of the orbital evolution. The second and third time derivatives of the quadrupoles are needed for (39) and (49). Using the angular velocity:

$$\omega = \frac{[(m_1 + m_2)a(1 - e^2)]^{1/2}}{d^2} \quad (53)$$

one finds the second derivatives to be:

$$\begin{aligned} \frac{d^2 Q_{xx}}{dt^2} &= -\gamma(4 \cos(2\phi) + e(3 \cos(\phi) + \cos(3\phi))), \\ \frac{d^2 Q_{yy}}{dt^2} &= \gamma(4 \cos(2\phi) + e(4e + 7 \cos(\phi) + \cos(3\phi))), \\ \frac{d^2 Q_{xy}}{dt^2} &= \frac{d^2 Q_{yx}}{dt^2} = -2\gamma \sin(\phi)(4 \cos(\phi) + e(3 + \cos(2\phi))), \end{aligned} \quad (54)$$

where γ defined as:

$$\gamma = \frac{m_1 m_2}{2a(1 - e^2)}. \quad (55)$$

The third derivatives evaluate to:

$$\begin{aligned} \frac{d^3 Q_{xx}}{dt^3} &= \beta(1 + e \cos \phi)^2 (2 \sin 2\phi + 3e \sin \phi \cos^2 \phi), \\ \frac{d^3 Q_{yy}}{dt^3} &= -\beta(1 + e \cos \phi)^2 (2 \sin 2\phi + e \sin \phi (1 + 3 \cos^2 \phi)), \\ \frac{d^3 Q_{xy}}{dt^3} &= \frac{d^3 Q_{yx}}{dt^3} = \\ &= -\beta(1 + e \cos \phi)^2 (2 \cos 2\phi - e \cos \phi (1 - 3 \cos^2 \phi)), \end{aligned} \quad (56)$$

with β defined as:

$$\beta^2 = \frac{4m_1^2 m_2^2 (m_1 + m_2)}{a^5 (1 - e^2)^5}. \quad (57)$$

The time derivative of the monopole $\partial_t M$ is also needed for eccentric binaries:

$$\partial_t M = -\frac{1}{2} (m_1 \partial_t v_1^2 + m_2 \partial_t v_2^2) = \frac{1}{2} \beta e \sin \phi (1 + e \cos \phi)^2. \quad (58)$$

The energy therefore radiates at the rate:

$$\partial_t E = -\frac{1}{15} \beta^2 (1 + e \cos \phi)^4 (4 + 2e^2 + 8e \cos \phi + 2e^2 \cos^2 \phi), \quad (59)$$

and likewise for the angular momentum:

$$\partial_t L_z = -\frac{2}{15} \beta \gamma (1 + e \cos \phi)^3 (8 - 2e^2 + 12e \cos \phi + 6e^2 \cos^2 \phi). \quad (60)$$

In general relativity the gravitational wave energy can't be localized at individual points in space, and therefore the expressions for the dE/dt and dL_z/dt need to be averaged over an orbit. While the energy can be localized in Nordström's theory, we will also average (59) and (60) in order to directly compare with general relativity. This is not a bad approximation since the orbital parameters evolve even more slowly than in GR. We find:

$$\langle \dot{E} \rangle = -\frac{16}{15} \frac{m_1^2 m_2^2 (m_1 + m_2)}{a^5 (1 - e^2)^{7/2}} \left[1 + \frac{13}{4} e^2 + \frac{7}{16} e^4 \right] \quad (61)$$

which is similar to the value given by Peters [27] for general relativity (differing only in the coefficients):

$$\langle \dot{E} \rangle = -\frac{32}{5} \frac{m_1^2 m_2^2 (m_1 + m_2)}{a^5 (1 - e^2)^{7/2}} \left[1 + \frac{73}{24} e^2 + \frac{37}{96} e^4 \right]. \quad (62)$$

Likewise for the angular momentum we average to find:

$$\langle \dot{L}_z \rangle = -\frac{16 m_1^2 m_2^2 (m_1 + m_2)^{1/2}}{15 a^{7/2} (1 - e^2)^2} \left[1 + \frac{7}{8} e^2 \right], \quad (63)$$

which again is one sixth the value found in general relativity.

Finally, by using

$$a = -m_1 m_2 / 2E, \quad (64)$$

$$L^2 = m_1^2 m_2^2 a (1 - e^2) / (m_1 + m_2) \quad (65)$$

$\langle \dot{E} \rangle$ and $\langle \dot{L}_z \rangle$ can be converted into rates of change for the semi-major axis $\langle \dot{a} \rangle$ and eccentricity $\langle \dot{e} \rangle$:

$$\left\langle \frac{da}{dt} \right\rangle = -\frac{32 m_1 m_2 (m_1 + m_2)}{15 a^3 (1 - e^2)^{7/2}} \left[1 + \frac{13}{4} e^2 + \frac{7}{16} e^4 \right], \quad (66)$$

and

$$\left\langle \frac{de}{dt} \right\rangle = -\frac{18 m_1 m_2 (m_1 + m_2)}{5 a^4 (1 - e^2)^{5/2}} e \left[1 + \frac{7}{18} e^2 \right]. \quad (67)$$

In the zero eccentricity case the semi-major axis integrates to:

$$a(t) = \left(a^4(0) - \frac{128}{15} m_1 m_2 (m_1 + m_2) t \right)^{1/4}. \quad (68)$$

Reproducing this 1/4 power law inspiral, similar to the expression found by Peters and Mathews for GR, is a major test of the Nordström simulation.

We also simulate binaries that retain some eccentricity e . Equations (66) and (67) can be combined to directly compare how a and e evolve:

$$\left\langle \frac{da}{de} \right\rangle = \frac{16}{27} \frac{a}{e(1 - e^2)} \frac{1 + \frac{13}{4} e^2 + \frac{7}{16} e^4}{1 + \frac{7}{18} e^2}. \quad (69)$$

An eccentric Nordström binary will therefore circularize as it evolves. Reproducing this rate of circularization, and the rate of precession given in (18), are the major tests of eccentric binaries in our numerical simulation.

III. NUMERICAL METHODS

A. Co-rotating Coordinates and the Weak Radiation Reaction Approximation

The field equation (5) needs to be finite differenced to simulate a binary system in Nordström's theory. We begin by rewriting the wave equation $-\partial_t^2 \varphi + \nabla^2 \varphi$ in a corotating spherical coordinate system. The corotating azimuthal angle $\bar{\phi}$ is given in terms of the original by: $\bar{\phi} = \phi - \Omega(t)$ (with $\Omega(t) = \int_0^t \omega(t') dt'$ and t , r , and θ remaining unchanged) where $\omega(t)$ always instantaneously

matches the binary's angular velocity. The differential equation becomes (dropping the bar notation):

$$-\partial_t^2 \varphi + \dot{\omega} \partial_\phi \varphi + 2\omega \partial_t \partial_\phi \varphi - \omega^2 \partial_\phi^2 \varphi + \nabla^2 \varphi = -4\pi(1 + \varphi)^3(\rho(1 + \varepsilon) - 3p). \quad (70)$$

Spherical harmonics are used to split this 3+1 differential equation into a set of 1+1 radial equations, one for each l and m term:

$$-\partial_t^2 \varphi_{lm} + im\dot{\omega} \varphi_{lm} + 2im\omega \partial_t \varphi_{lm} + m^2 \omega^2 \varphi_{lm} + \frac{\partial_r [r^2 \partial_r \varphi_{lm}]}{r^2} - \frac{l(l+1) \varphi_{lm}}{r^2} = 4\pi S_{lm}(t, r), \quad (71)$$

where the source term is also decomposed:

$$S_{lm}(t, r) = \int d\Omega Y_{lm}^*(\theta, \phi) [(1 + \varphi)^3(\rho(1 + \varepsilon) - 3p)]. \quad (72)$$

We have written a spherical harmonics package as part of the code in order to evaluate (72) and also synthesize the field φ from its φ_{lm} components. We will use (71) to simulate binaries that retain some degree of eccentricity.

For binaries that are in quasi-circular orbits, we make the Weak Radiation Reaction (WRR) approximation, which is based on the presence of two timescales: the fast orbital motion characterized by ω (with period $T \sim \omega^{-1}$), and the longer radiation reaction timescale τ . For a binary with separation d the ratio of these timescales goes as $\tau/T \sim (d/M)^{5/2}$. Thus there is a hierarchy of scales among the time derivatives:

$$\frac{\partial}{\partial t^2} \sim \frac{1}{\tau^2}, \quad \omega \frac{\partial}{\partial t} \sim \dot{\omega} \sim \frac{1}{T\tau}, \quad \omega^2 \frac{\partial}{\partial \phi^2} \sim \frac{1}{T^2}. \quad (73)$$

The second time derivative term is the smallest, and is dropped when making the WRR approximation, giving a first order in time differential equation (which resembles the 1-D Schrödinger equation):

$$\partial_t \varphi_{lm} = \frac{i}{2m\omega} \left[\frac{\partial_r [r^2 \partial_r \varphi_{lm}]}{r^2} + (m^2 \omega^2 + im\dot{\omega} - \frac{l(l+1)}{r^2}) \varphi_{lm} - 4\pi S_{lm}(t, r) \right] \quad (74)$$

for the $m \neq 0$ terms and

$$\frac{\partial_r [r^2 \partial_r \varphi_{l0}]}{r^2} - \frac{l(l+1)}{r^2} \varphi_{l0} - 4\pi S_{l0}(t, r) = 0 \quad (75)$$

for the time independent $m = 0$ terms.

To solve for the initial data for the Cauchy evolution the single time derivative terms in equation (74) are dropped, giving:

$$\frac{\partial_r [r^2 \partial_r \varphi_{lm}]}{r^2} + \left(m^2 \omega^2 - \frac{l(l+1)}{r^2} \right) \varphi_{lm} - 4\pi S_{lm}(t, r) = 0. \quad (76)$$

This leaves the boundary conditions. The inner boundary is given by setting the radial derivative of the φ_{lm} terms to zero:

$$\partial_r \varphi_{lm} = 0. \quad (77)$$

At the outer boundary the Sommerfeld outgoing wave boundary condition is used, which has the following form in the co-rotating reference frame:

$$\partial_t \varphi_{lm} = im\omega \varphi_{lm} - (1/r) \varphi_{lm} - \partial_r \varphi_{lm}. \quad (78)$$

The binaries are first modeled in a quasi-circular orbit (with the expected inspiral given by (68)) with equations (74) and (75) used to evolve the field φ . As noted equation (74) closely resembles the Schrödinger equation, so it is finite differenced using the Crank-Nicholson method (see e.g. [30]).

The hyperbolic equation (71) needs to be finite differenced for inspirals that retain some eccentricity. Given the success we have in evolving (74) with Crank-Nicholson, we devise a modified Crank-Nicholson for (71):

$$\begin{aligned} & -(\varphi_i^{N+1} - 2\varphi_i^N + \varphi_i^{N-1}) + im\omega \Delta t (\varphi_i^{N+1} - \varphi_i^{N-1}) = \\ & \quad (79) \\ & \frac{\Delta t^2}{2} \left(-\frac{(\varphi_{i+1}^{N+1} - 2\varphi_i^{N+1} + \varphi_{i-1}^{N+1})}{\Delta r^2} - \frac{(\varphi_{i+1}^{N+1} - \varphi_{i-1}^{N+1})}{r\Delta r} \right. \\ & \quad \left. + \left(\frac{l(l+1)}{r^2} - m^2\omega^2 - im\dot{\omega} \right) \varphi_i^{N+1} \right) \\ & + \frac{\Delta t^2}{2} \left(-\frac{(\varphi_{i+1}^{N-1} - 2\varphi_i^{N-1} + \varphi_{i-1}^{N-1})}{\Delta r^2} - \frac{(\varphi_{i+1}^{N-1} - \varphi_{i-1}^{N-1})}{r\Delta r} \right. \\ & \quad \left. + \left(\frac{l(l+1)}{r^2} - m^2\omega^2 - im\dot{\omega} \right) \varphi_i^{N-1} \right) \\ & \quad + 2\pi \Delta t^2 (S_i^{N+1} + S_i^{N-1}). \end{aligned}$$

We find that this balanced implicit method also allows for fast, stable, and accurate field evolutions.

B. Numerical Tests

We use a mixture of finite difference and pseudo-spectral methods, and these need to be tested first before evolving the full system. A useful test case is provided by the Newtonian system, with the inhomogeneous wave equation reducing to Poisson's equation:

$$\nabla^2 \varphi = 4\pi\rho, \quad (80)$$

and the acceleration is given by $F = ma$:

$$\frac{d^2 x_a^i}{dt^2} = \frac{1}{M_a} \int_a \rho \partial_i \varphi d^3x. \quad (81)$$

Equation (80) can be split into its spherical harmonic components by dropping the $m^2\omega^2\varphi_{lm}$ term from equation (76):

$$\frac{\partial_r [r^2 \partial_r \varphi_{lm}]}{r^2} - \frac{l(l+1)}{r^2} \varphi_{lm} + 4\pi S_{lm}(t, r) = 0, \quad (82)$$

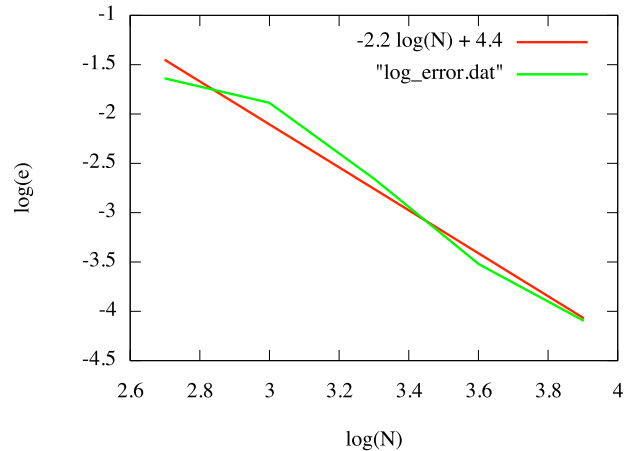


FIG. 1: Plotted is the \log_{10} of the error $e = \sup |\varphi_{Newton}/\varphi - 1|$ against the \log_{10} of the number of radial grid points N . A linear fit gives a slope of -2.2 ± 0.2 , i.e. second order convergence. The lowest resolution grid uses $N = 500$ radial grid-points and L and M values up to 25. This is then doubled four times up to resolution with $N = 8000$ radial grid points and L and M values up to 400.

with the source terms given by $S_{lm}(t, r) = \int d\Omega Y_{lm}^*(\theta, \phi) \rho(t, r, \theta, \phi)$. Equation (82) is then finite differenced in the standard second order manner. In order to check the convergence of the numerical solution we choose a matter distribution for the stars given by $\rho(r) = \rho_0(1 - r^2/R^2)$ (with some central density ρ_0 and radius R) which allows for an exact analytical solution for φ . After solving for the φ_{lm} components based on this source and then synthesizing the field φ , we find that our numerical solution converges at second order to the analytical solution, as shown in figure (1).

The Newtonian system presents a second test in addition to the convergence of the field: the integral in equation (81) must also converge to the expected inverse square law. Note also that we are already using a “hydro-without-hydro” type of approximation: the matter is described by a rigid density profile, so that only the acceleration of the center of mass needs to be determined. We find that accurately resolving this acceleration is somewhat involved in a spherical coordinate system. For a given resolution, and using second order methods, we generally find that the solution for the field (80) is much more accurate than the result for the acceleration (81). The error in the computed acceleration also grows quite quickly as the separation increases. The error does converge to zero as the resolution is increased, but inconveniently high resolutions are needed to reduce it to acceptable values.

This inconvenience arises because (81) includes the gradient of the star’s self field. The Newtonian self force integrates to zero analytically, but numerically there will be some small residue. Furthermore, the amplitude of the self field is much larger the $1/r$ contribution from the

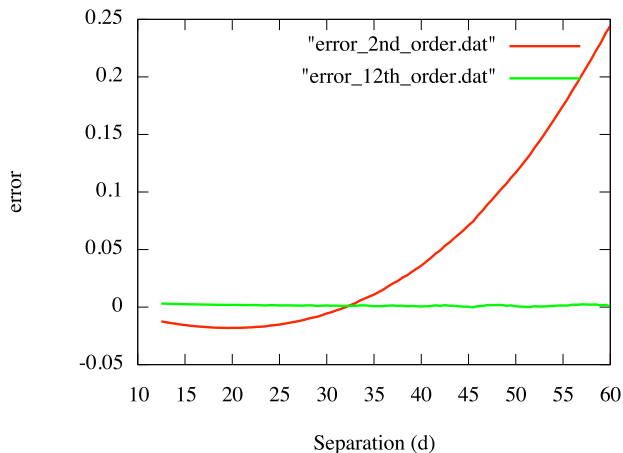


FIG. 2: Plotted is the error $= (a_r)/(1/d^2) - 1$ of the radial acceleration (compared to the expected Newtonian inverse square law with a mass of 1) as a function of the separation d for the 2nd order and 12th order derivative methods. The standard 2nd order accurate method gives an error of 25 percent for a separation of $60M$ (for a particular grid resolution), while the 12th order method gives an error of ~ 0.3 percent, which is the same accuracy the field is resolved to at this separation.

other star, so a small percent error in calculating its gradient can swamp the correct $1/r^2$ contribution from the other star, especially as the separation increases and the resolution inside the stars decreases (for a fixed spherical grid).

Experimentation shows that the error grows almost as quickly if the analytic solution for φ is inserted into the mesh and then finite differenced to calculate (81). However, if the analytical derivatives $\partial_i\varphi$ are inserted into (81) then the result for the acceleration is much more accurate – now comparable to the accuracy of (80). We thus need much more accurate derivatives, which are available through higher order methods. Experimentally, each increase in the order of the derivatives gave better results (as compared to the analytical solutions), so we used 12th order accurate derivatives, given by:

$$\begin{aligned} \partial_i\varphi \simeq \frac{1}{27720\Delta x} [& 5\varphi_{i-6} - 72\varphi_{i-5} + 495\varphi_{i-4} \\ & - 2200\varphi_{i-3} + 7425\varphi_{i-2} - 23760\varphi_{i-1} \\ & + 23760\varphi_{i+1} - 7425\varphi_{i+2} + 2200\varphi_{i+3} \\ & - 495\varphi_{i+4} + 72\varphi_{i+5} - 5\varphi_{i+6}]. \end{aligned} \quad (83)$$

The resulting improvement in the acceleration is shown in figure (2). Note that we do not claim to have a 12th order accurate code, as the field φ is still solved for with 2nd order accurate implicit methods. However, these higher order derivatives do allow the net accelerations computed in (81) to have the same level of accuracy as the solution for φ .

The next test is to promote the Laplacian operator in

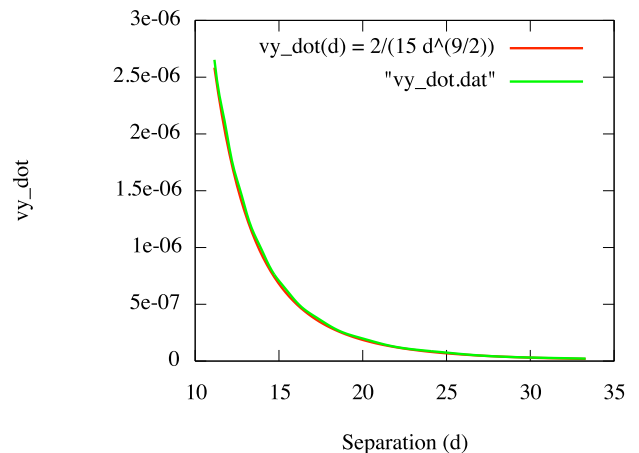


FIG. 3: Plot of the measured acceleration dv^y/dt (i.e. in the ϕ direction) as a function of separation, which closely matches the expectation given in 85.

equation (80) to a wave operator:

$$\square\varphi = 4\pi\rho. \quad (84)$$

The spherical harmonic decomposition for this in corotating coordinates was given in (71) and the initial data is found by solving (76). The homogeneous version of (76) is solved by the Bessel and Neumann functions $j_l(m\omega r)$ and $\eta_l(m\omega r)$, or in the case of the Sommerfeld boundary condition (78), by an outgoing wave spherical Hankel function. At large r this asymptotically approaches a sinusoidal function of frequency $m\omega$ with a $1/r$ envelope. Our finite difference code correctly reproduces this asymptotic behavior.

This simple wave equation system also provides another test of the net acceleration of the center of mass. For this test we retain the Newtonian equation (81) to calculate accelerations based on the field φ . In Newtonian language, the wave equation $\square\varphi$ gives rise to a radiation reaction potential $\Phi^{(react)}$ (when driven by the orbital motion of the compact bodies). This potential $\Phi^{(react)}$ results in a drag force acting on the stars, causing the orbit to decay in a manner that closely matches the full theory. A quadrupole calculation similar to the full Nordström theory version finds that the orbit decays at the rate: $\dot{d} = -(64/15)m_a^3/d^3$ where d is the separation and $m_a = m_b$ is the mass of the equal mass stars. Let the two stars be instantaneously aligned along the x-axis in a Cartesian plane, at $\pm d/2$ away from the origin, with Newtonian velocities $v^y = \pm \dot{y}(m_a/2d)^{1/2}$. The gradient of $\Phi^{(react)}$ then gives an acceleration opposite to the velocity (i.e., in the ϕ direction):

$$\ddot{v}^y = (1/15)m_a^{7/2}/(d/2)^{9/2}, \quad (85)$$

thereby causing a quasi-circular inspiral. The code accurately reproduces the inverse nine-halves scaling of this acceleration, as shown in Figure (3), where we have set $m_a = 1/2$ (so that the total mass is 1).

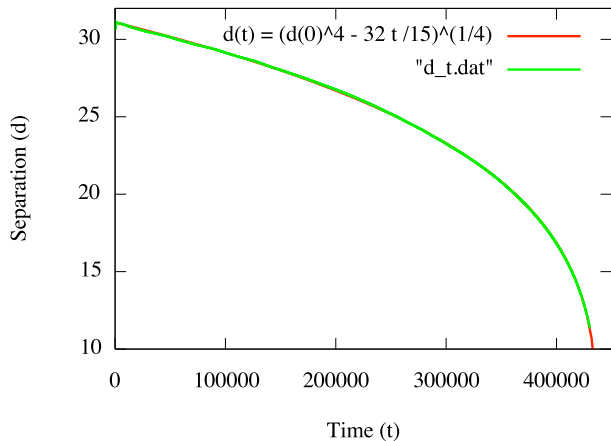


FIG. 4: Separation d as a function of time for a quasi-circular inspiral. The inspiral closely matches the $1/4$ power law result given in (68).

IV. MODELING NORDSTRÖM'S THEORY

With the initial tests passed we can now simulate Nordström theory. Again we solve for the initial data with (76), but we do not decompose the source as we did in (72). Instead we rewrite the source term using the conserved density ρ^* , finding:

$$S_{lm}(t, r) = \int d\Omega Y_{lm}^*(\theta, \phi) [\sqrt{1 - v^2} \rho^* (1 + \varepsilon - 3p/\rho)]. \quad (86)$$

This removes much of the nonlinearity from the equation of motion for the field. We find ε and $-3p/\rho$ using ρ^* (which is held constant under the hydro-without-hydro approximation), and the value of φ .

We first model quasi-circular inspirals by making use of the WRR approximation. Initial data is found by starting with a circular Keplerian binary, and then iteratively tuning the orbital parameters to reduce the initial eccentricity. The field is then evolved forward in time via (74), which is finite differenced with the Crank-Nicholson scheme. Note that it is crucial to also time average the source $S_{lm}(t, r)$ in the Crank-Nicholson scheme, as otherwise the source and field will be a half time step out of sync which results in spurious accelerations.

After each time step the field $\varphi(r, \theta, \phi)$ is synthesized from its spherical harmonic components and used to solve for the acceleration using a discretized combination of (14) and (15). As noted, 12th order finite differencing is used for the derivatives of φ so that the net acceleration is accurate. The components of equation (15) are also expanded out in the corotating reference frame. The corotating coordinate transformation adds shift vector like terms to the metric which in turn leads to new terms in the sum of connection coefficients $\Gamma_{\alpha\beta}^j v^\alpha v^\beta$. These additions effectively add a centripetal force, so that when the correct ω is found (via iterative testing) the stars will

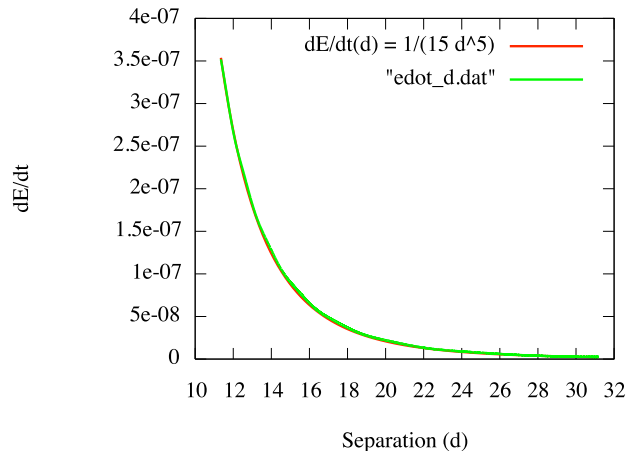


FIG. 5: Plot of the rate of energy loss of the binary dE/dt as a function of the separation d , compared to the theoretical value given in (61), where $m_1 = m_2 = 0.5$ and $e = 0$.

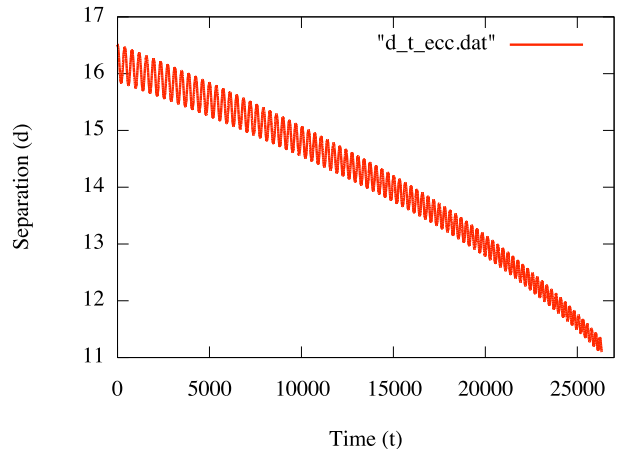


FIG. 6: Separation d as a function of time for a binary with an initial eccentricity of $e \sim 0.021$.

be nearly at rest in the co-rotating frame (except for the slow merger due to the radiation reaction).

The masses of the stars are set to $m_a = m_b = 1/2$ for both the quasi-circular and eccentric simulations. An initial central density of $\rho_c^* \sim 3.72 \times 10^{-4}$ and polytropic parameters $\Gamma = 5/3$ and $\kappa = 7.29$ are picked to give a compactness of $m_a/R_a = 0.1$. The stars are then rescaled in the simulation to give a total mass of 1, so that each star has a radius of $5M$. The outer radial boundary is set to $r_{outer} = 560M$, which places it in the wave zone for an initial separation of $31M$. The radial grid spacing is $\Delta r = 0.4M$, and spherical harmonic modes up to $l = m = 80$ are used (in general the discretization is chosen so that there is comparable resolution in the angular and radial directions). As we use Crank-Nicholson to evolve (74) for the quasi-circular case we can utilize a time step of $\Delta t = 6.0M$. This is much larger than the value given

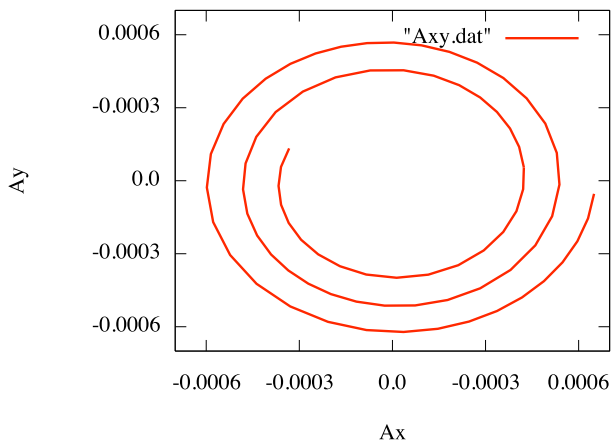


FIG. 7: Plot of the Runge Lenz vector \mathbf{A} as it evolves, which demonstrates that binary precesses about 2.5 times over the course of the inspiral. The circularization of the binary can also be seen as the magnitude of \mathbf{A} drops by about a factor of two.

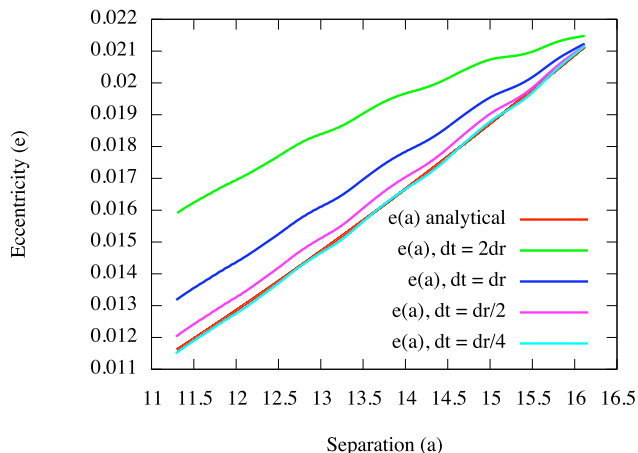


FIG. 8: Plot of the eccentricity e as a function of the semi-major axis a for simulations with a time step Δt ranging from 2.0 to 0.25 Δr vs. the analytical expectation from (69).

by the Courant-Friedrichs-Lewy (CFL) condition, but is sufficient to resolve the slow evolution of the system on the radiation reaction timescale. A large time step also proves to be stable for eccentric binaries, but in this case there is dynamical motion on the shorter orbital time scale, and experimentation shows that time steps similar to the CFL condition are needed in order to get accurate results.

The binary separation as a function of time for the quasi-circular evolution is given in Figure (4). The initial separation is set to be $31M$ and the stars then inspiral to a separation of $11M$ (i.e. almost to merger) over the course of ~ 600 orbits. The inspiral closely matches the $1/4$ power law (68) predicted by the semi-analytical calculation. In Figure (5) we plot the rate of energy loss as

measured directly at the outer shell of the domain. We find a close match to the analytical prediction given in (61). The energy contained in the volume of the computational domain is also tracked using (6) and found to decrease in sync with the energy flux through the outer boundary. The quasi-circular inspiral therefore closely matches the analytical expectations.

Next we examine binaries that retain a small amount of eccentricity. The WRR approximation is dropped and the field is evolved with the modified Crank-Nicholson scheme given in (79). We select a value of ω which gives the binary a small amount of eccentricity ($e \sim 0.02$) at an initial separation of $a \sim 16M$. With this small value of e the binary decays only slightly faster than a quasi-circular binary with the same semi-major axis. The system circularizes noticeably over the evolution (finishing with $e \sim 0.01$) as can be seen in Fig. (6).

We first compare the rate of precession to the analytical profile (18) given by Post Newtonian calculations. We find that the code matches this expectation closely: for the chosen initial data the binary precesses about 5π radians over the course of dozens of orbits as the separation d decreases from $16M$ to $11M$. This precession can be seen by fitting the Runge-Lenz vector \mathbf{A} to the binary's orbital parameters (and then averaging over an orbit to remove any orbital timescale artifacts). \mathbf{A} points along the semi-major axis, and is proportional to the eccentricity. It therefore compactly displays both the precession and circularization of a binary, as shown in Figure (7).

The gradual circularization of the binary can also be seen in Figure (8), where an extracted value for $e(a)$ (for simulations with a range of time steps) is compared to the result found by integrating the analytical form in (69). The slow secular evolution of e is quite sensitive to accumulating errors, and we find that the time step needs to be reduced to $\Delta t \sim \Delta r/4$ in order to get accurate results.

V. CONCLUSIONS

The numerical techniques we have developed work well in simulating binary inspirals in Nordström's theory. The co-rotating spherical coordinate system is quite sensitive to the 2.5 PN order radiation reaction force, and is well suited to conserving angular momentum, allowing for accurate evolution of inspirals over many orbits (~ 600 in the case of the quasi-circular inspiral). The code demonstrates this, as it accurately matches the analytic predictions we made for Nordström's theory, from the $1/4$ power law profile for a quasi-circular inspiral and the corresponding rate of energy loss, to the rate of precession and circularization of an eccentric binary.

As a side benefit we find that Nordström's second theory is a useful laboratory for developing computational techniques for numerical relativity. It is a fully relativistic metric theory, and yet has fairly simple field equations which can be put in a nearly linear form. Furthermore

the theory follows the SEP and thus stars move on Keplerian orbits to lowest order, and there are no star-crushing effects.

Our main goal is to use our corotating spherical coordinates framework to model the late inspirals of binaries

in GR. We explore a modification of a generalized harmonic formulation of the Einstein equations to this end in [31]. Given the success we have had in applying it to Nordström binaries, we feel confident that it should allow for fast, long and accurate simulations in GR as well.

-
- [1] T. Nakamura, K. Oohara, and Y. Kojima. General Relativistic Collapse to Black Holes and Gravitational Waves from Black Holes. *Prog. Theor. Phys. Suppl.*, 90:1–218, 1987.
- [2] M. Shibata and T. Nakamura. Evolution of three-dimensional gravitational waves: Harmonic slicing case. *Phys. Rev.*, D52:5428–5444, 1995.
- [3] Thomas W. Baumgarte and Stuart L. Shapiro. On the numerical integration of Einstein’s field equations. *Phys. Rev.*, D59:024007, 1999.
- [4] M. Campanelli, C. O. Lousto, P. Marronetti, and Y. Zlochower. Accurate evolutions of orbiting black-hole binaries without excision. *Phys. Rev. Lett.*, 96:111101, (2006), gr-qc/0511048.
- [5] J. G. Baker, J. Centrella, D. I. Choi, M. Koppitz, and J. van Meter. Gravitational wave extraction from an inspiraling configuration of merging black holes. *Phys. Rev. Lett.*, 96:111102, (2006), gr-qc/0511103.
- [6] David Garfinkle. Harmonic coordinate method for simulating generic singularities. *Phys. Rev.*, D65:044029, 2002.
- [7] F. Pretorius. Evolution of binary black hole spacetimes. *Phys. Rev. Lett.*, 95:121101, (2005), gr-qc/0507014.
- [8] Baker J. G., M. Campanelli, F. Pretorius, and Y. Zlochower. Comparisons of binary black hole merger waveforms. (2007), gr-qc/0701016.
- [9] Mark Hannam. Status of black-hole-binary simulations for gravitational-wave detection. *Class. Quant. Grav.*, 26:114001, 2009.
- [10] J. G. Baker, J. R. van Meter, S. T. McWilliams, J. Centrella, and B. J. Kelly. Consistency of post-newtonian waveforms with numerical relativity. (2006), gr-qc/0612024.
- [11] Jocelyn S. Read and et al. Measuring the neutron star equation of state with gravitational wave observations. *Phys. Rev.*, D79:124033, 2009.
- [12] M. A. Scheel, H. P. Pfeiffer, L. Lindblom, L. E. Kidder, O. Rinne, and S. A. Teukolsky. Solving einstein’s equations with dual coordinate frames. *Phys. Rev. D*, 74:104006, (2006), arXiv:gr-qc/0607056v2.
- [13] M. A. Scheel, M. Boyle, T. Chu, L. E. Kidder, K. D. Matthews, and H. P. Pfeiffer. High-accuracy waveforms for binary black hole inspiral, merger, and ringdown. (2008), arXiv:0810.1767v1 [gr-qc].
- [14] Bela Szilagyi, Lee Lindblom, and Mark A. Scheel. Simulations of Binary Black Hole Mergers Using Spectral Methods. *Phys. Rev.*, D80:124010, 2009.
- [15] Marsha J. Berger and Joseph Olinger. Adaptive Mesh Refinement for Hyperbolic Partial Differential Equations. *J. Comput. Phys.*, 53:484, 1984.
- [16] L. Lehner, S. L. Liebling, and O. Reula. Amr, stability and higher accuracy. *Class. Quantum Grav.*, 23:S421–S446, (2006), arXiv:gr-qc/0510111v1.
- [17] P.R. Brady, J.D.E. Creighton, and K.S. Thorne. Computing the merger of black-hole binaries: the ibbh problem. *Phys. Rev. D.*, 58:061501, (1998),gr-qc/9804057.
- [18] T.W. Baumgarte, S.A. Hughes, and S.L. Shapiro. Evolving einstein’s field equations with matter: The “hydro without hydro” test. *Phys. Rev. D*, 60:087501, (1999),gr-qc/9902024.
- [19] J. R. Driscoll and D. M. Jr. Healy. Computing fourier transforms and convolutions on the 2-sphere. *Advan. App. Math.*, 15:202–250, (1994).
- [20] B. K. Alpert and V. Rokhlin. A fast algorithm for the evaluation of legendre expansions. *SIAM J. Sci. Stat. Comp.*, 12:158–179, (1991).
- [21] D. M. Jr. Healy, D. N. Rockmore, P. J. Kostelec, and S. Moore. Ffts for the 2-sphere-improvements and variations. *J. Four. An. App.*, 9:341–385, (2003).
- [22] S. L. Shapiro and S. A. Teukolsky. Scalar gravitation: A laboratory for numerical relativity. *Phys. Rev. D*, 47:1529, 1993.
- [23] K. Watt and C. W. Misner. Relativistic scalar gravity: A laboratory for numerical relativity. (1999),gr-qc/9910032.
- [24] W. T. Ni. Theoretical frameworks for testing relativistic gravity. iv. a compendium of metric theories of gravity and their post-newtonian limits. *Astrophysical Journal* 176:769–796, 1972.
- [25] K. Nordtvedt. Testing relativity with laser ranging to the moon. *Phys. Rev.*, 170:1186–1187, 1968.
- [26] P. C. Peters and J. Mathews. Gravitational radiation from point masses in a keplerian orbit. *Phys. Rev.* 131,435, (1963).
- [27] P. C. Peters. Gravitational radiation and the motion of two point masses. *Phys. Rev.* 136,1224, (1964).
- [28] A. G. Wiseman. The central density of neutron stars in close binaries. *Phys. Rev. Lett.*, 79,1189–1192, (1997), gr-qc/9704018.
- [29] C. M. Will. *Theory and Experiment in Gravitational Physics Revised Edition*. Cambridge University Press, (1993).
- [30] W. H. Press, S. A. Teukolsky, Vetterling W. T., and B. P. Flannery. *Numerical Recipes in C 2nd Ed*. Cambridge University Press, (1992).
- [31] T. M. Garrett. A simple, direct finite differencing of the einstein equations. (2009), arXiv:0902.0803.